Assessing Impacts of Integrating MODIS Vegetation Data in the Weather Research and Forecasting (WRF) Model Coupled to Two Different Canopy-Resistance Approaches

ANIL KUMAR

NASA Goddard Space Flight Center, Greenbelt, and Earth System Science Interdisciplinary Center, College Park, Maryland, and Department of Earth, Atmospheric and Planetary Sciences, Purdue University, West Lafayette, Indiana

FEI CHEN AND MICHAEL BARLAGE

National Center for Atmospheric Research, Boulder, Colorado*

MICHAEL B. EK

National Centers for Environmental Prediction, Camp Springs, Maryland

DEV NIYOGI

Department of Earth, Atmospheric and Planetary Sciences, Purdue University, West Lafayette, Indiana

(Manuscript received 26 July 2013, in final form 30 December 2013)

ABSTRACT

The impact of 8-day-averaged data from the Moderate Resolution Imaging Spectroradiometer (MODIS) sensor—namely, the 1-km leaf area index, absorbed photosynthetic radiation, and land-use data—is investigated for use in the Weather Research and Forecasting (WRF) model for regional weather prediction. These high-resolution, near-real-time MODIS data are hypothesized to enhance the representation of land–atmosphere interactions and to potentially improve the WRF model forecast skill for temperature, surface moisture, surface fluxes, and soil temperature. To test this hypothesis, the impact of using MODIS-based land surface data on surface energy and water budgets was assessed within the ''Noah'' land surface model with two different canopy-resistance schemes. An ensemble of six model experiments was conducted using the WRF model for a typical summertime episode over the U.S. southern Great Plains that occurred during the International H_2O Project (IHOP_2002) field experiment. The six model experiments were statistically analyzed and showed some degree of improvement in surface latent heat flux and sensible heat flux, as well as surface temperature and moisture, after land use, leaf area index, and green vegetation fraction data were replaced by remotely sensed data. There was also an improvement in the WRF-simulated temperature and boundary layer moisture with MODIS data in comparison with the default U.S. Geological Survey land-use and leaf area index inputs. Overall, analysis suggests that recalibration and improvements to both the input data and the land model help to improve estimation of surface and soil parameters and boundary layer moisture and led to improvement in simulating convection in WRF runs. Incorporating updated land conditions provided the most notable improvements, and the mesoscale model performance could be further enhanced when improved land surface schemes become available.

1. Introduction

The interaction between the surface layer and lower atmospheric layers is important for weather and climate models. The role of land–atmosphere interactions becomes even more important over a warm, moist surface covered by different vegetation types (Ek et al. 2003; Dirmeyer et al. 2010). The value of improving land

* The National Center for Atmospheric Research is sponsored by the National Science Foundation.

Corresponding author address: Dr. Anil Kumar, Hydrological Science Branch (Code-614.3), NASA/GSFC, Greenbelt, MD 20771.
E-mail: anil.kumar@nasa.gov

DOI: 10.1175/JAMC-D-13-0247.1

© 2014 American Meteorological Society

surface models to enhance operational forecasts is recognized by the different numerical weather prediction (NWP) centers (e.g., Beljaars et al. 1996; Betts et al. 1997; Chen et al. 1997; Ek et al. 2003). A variety of land surface models have been developed that incorporate the response of land surface feedbacks contributed from changes in soil moisture, surface albedo, surface roughness length, surface moisture, and the evapotranspiration–rain relation [see Pitman (2003) and Pielke et al. (2011) for a review].

In this study, the Weather Research and Forecasting (WRF) model coupled with the "Noah" land surface model (LSM) is used. This LSM adopts Penman potential evaporation (Mahrt and Ek 1984), a four-layer soil model (Mahrt and Pan 1984), and the canopy/transpiration representation of Pan and Mahrt (1987). The Noah LSM is further improved by Chen et al. (1996), who introduced the Jarvis canopy-resistance approach following Noilhan and Planton (1989) and Jacquemin and Noilhan (1990). The details of the LSM are discussed in Chen and Dudhia (2001a). Land surface properties [e.g., vegetation, leaf area index (LAI), green vegetation fraction (GVF), and albedo] in the Noah model significantly control surface energy partitioning and moisture to the atmospheric boundary layer. Hence, these inputs can have an impact on convection initiation and precipitation (Chen and Dudhia 2001a,b; Trier and Davis 2005; Holt et al. 2006; Niyogi et al. 2006).

Prior results lead to a hypothesis that the weakness due to misrepresentation of vegetation greenness in the model can negatively impact convection and boundary layer moisture prediction. Some of the weaknesses in the current Noah LSM include 1) a low resolution of vegetation data, 2) climatologically based GVF, and 3) a constant LAI value. The evapotranspiration and soil moisture relation is directly linked to vegetation greenness, and biases are generally proportional to the vegetation greening (Vivoni et al. 2008).

The current dataset used in the Noah model is based on a 0.144° monthly climatological dataset derived from a 1992 Advanced Very High Resolution Radiometer (AVHRR) database; the LAI is considered to be vegetation dependent and was assigned a constant value for each vegetation type. Considering the merits of the advanced WRF model that provides simulations at a very high resolution (in the range of few kilometers), the GVF or LAI in the coarser resolution can negatively affect model results for finer-scale simulations. Hence, with high-resolution land cover, LAI and GVF data derived from the Moderate Resolution Imaging Spectroradiometer (MODIS) sensor can provide detailed vegetation information to the model on both spatial and temporal scales (Barlage at al. 2005; Miller et al. 2006; Hong et al. 2007; Wang et al. 2007). These MODIS vegetation variables and biophysical variables such as LAI and photosynthetically active radiation fraction (fPAR, which is an estimate of GVF; see Wood et al. 1998) were used here to estimate surface energy and the mass exchange process. This was done by putting satellite data products for LSMs into the operational WRF–Noah system. The LAI actively contributes to the surface heat and vapor transfer through estimation of canopy resistance R_c, which describes the resistance of vapor flow through the transpiring vegetation and evaporation from the land surface (Niyogi and Raman 1997). While discussing the current results, the impact of introducing a photosynthesis-based resistance formulation called the Gas-Exchange Model (GEM; Niyogi et al. 2009) in the Noah model is also reviewed. In the experiments with the regional WRF model, the impact of new MODIS-based input parameters on regional, high-resolution modeling is also discussed.

There is growing evidence that the Jarvis-type approach should be replaced by a more interactive photosynthesis-based R_c scheme (Pitman 2003; Holt et al. 2006; Niyogi et al. 2009; Charusombat et al. 2010). It remains to be investigated whether the photosynthesis-based R_c model should be adopted or whether recalibrating the Jarvis-type model from the in situ and satellite datasets would be sufficient. The value of satellite land observations from new sensors will be reduced unless they can be effectively integrated in LSMs for operational weather forecast models.

Thus, the study objectives include 1) integration of new MODIS-based land fields (land use, leaf area index, and green vegetation fraction) in the Noah LSM, 2) understanding the effects of such integration on coupled simulations of both regional-scale water vapor and heat exchange in the Noah LSM, 3) evaluation of the new R_c parameterization schemes including a photosynthesis approach that links with new satellite-derived data, and 4) determining the advantage of introducing a photosynthesis-based R_c scheme in the "traditional" Jarvis-type representation in the Noah LSM. Section 2 introduces both the MODIS and U.S. Geological Survey (USGS) datasets and details our approach in testing the land-use, LAI, and GVF parameters.

2. MODIS and USGS land vegetation data: Land use, LAI, and GVF

The International Geosphere–Biosphere Programme's (IGBP) land-cover classification recognizes 17 vegetation types and includes 11 categories of natural vegetation, three classes of mosaic types, and three classes of non-vegetative lands (Friedl et al. 2002). Our study uses the

MODIS 1-km IGBP classification data developed at Boston University (Boston University 2012) but excludes the permanent wetland and cropland/natural vegetation mosaic and includes three new classes of tundra that were added by the National Centers for Environmental Prediction (NCEP). The level-4 MODIS global LAI and fPAR (assumed to be equivalent to GVF) are developed every 8 days at 1-km resolution on a sinusoidal grid. LAI is used directly by the Noah LSM in WRF, and fPAR can be used as a proxy for GVF (Chen et al. 2003; Liu et al. 2006; Gobron et al. 2010) when the normalized difference vegetation index is unavailable. These data were interpolated to a regular 0.01° geographic projection so that they could be used by the WRF Preprocessing System (WPS) and transferred to the WRF grid.

Figure 1 shows the comparison of the USGS and MODIS land-cover categories over the U.S. southern Great Plains (SGP). In this region, vegetation categories showed differences for the two land datasets, especially in the distribution of grassland, cropland, and savanna vegetation types. The major change was found across the savanna vegetation type; it is not present in the classification used in the MODIS land use and is presented as grassland instead. In a similar way, the patterns of grassland and cropland were also represented differently across this SGP region.

Within most land surface models, LAI and GVF are the sensitive input parameters (Rosero et al. 2010) and significantly control the surface heat flux; hence, we compared these parameters using the USGS and MODIS land-use maps shown in Fig. 2. Leaf area index is defined as the gridcell area of leaf surface per vegetation fraction of the grid area, and GVF is described using the fractional area of vegetation occupying a given pixel (Knote et al. 2009). Figures 2a and 2b show large differences between two GVF sources. MODIS GVF showed a difference of ~0.1 in the western part of the domain (i.e., the region between 103° and 100°W), whereas the central part of the model domain (i.e., between 100° and 99°W) shows MODIS values that were ~0.2 less than the USGS-based GVF. In the eastern part of the domain (96°–94°W), more significant differences were visible in the two GVF datasets, and the MODIS-based GVF had a more realistic distribution than its USGS counterpart. This is mainly because MODIS data are available in near–real time at 1-km resolution whereas USGS GVF is based on climatological information. The default LAI, found by referencing a lookup table (LUT), is dependent on the USGS vegetation classification (Fig. 2c). MODIS-based LAI is shown in Fig. 2d, where large differences in LAI distribution (~3–4) are seen over one-half of the model domain and are visible west of the center of the domain. The satellite-derived LAI was very different from the LUT-based LAI currently used in the WRF configuration. One of the advantages in using MODIS LAI is its ability to get high spatial resolution and temporally varying LAI and GVF information into NWP models. It is anticipated that doing this will ultimately improve the representation of vegetation and transpiration processes in the Noah land surface model.

3. Canopy-resistance parameterization schemes in the Noah land surface model

At this time, WRF–Noah adopts the Jarvis-type approach in parameterizing canopy resistance R_c. Through a detailed diagnosis of the operational Global Forecast System (GFS) and Nonhydrostatic Mesoscale Model (NMM) biases, NCEP scientists highlighted the uncertainty in specifying minimum stomatal resistance $R_{c,\min}$ and a constant LAI in the Jarvis formulation (Mitchell et al. 2005). These limitations can be addressed in the photosynthesis/carbon dioxide (CO_2)-based LSMs (Sellers et al. 1996a), which are next-generation schemes with biochemical responses that are explicitly coupled to both the atmosphere and surface to estimate CO_2, water vapor, and energy exchange (Farquhar et al. 1980; Collatz et al. 1991, 1992; Leuning 1995). The response from stomata and environmental feedback is sensitive to air temperature and is parameterized through a hydromechanical model involving epidermal and plant–water relations. These type of models have been mostly used in leaf/canopy-scale models (Baldocchi 1992; Nikolov et al. 1995; Buckley et al. 2003; Niyogi et al. 2006, 2009; Kumar et al. 2011) or for global/regional climate studies (Sellers et al. 1996b; Calvet et al. 1998; Cox et al. 1999; Eastman et al. 2001; Zhan et al. 2003) and in a somewhat limited sense within the mesoscale modeling framework (Holt et al. 2006; Niyogi et al. 2007; Chang et al. 2009). The Ball–Berry and Jarvis models were evaluated under various soil moisture conditions over different land types using land data assimilation systems, and it was concluded that the Ball–Berry model is more sensitive under both dry and wet soil conditions (Kumar et al. 2011). Niyogi and Raman (1997). Medlyn et al. (2001) studied the Jarvis and Ball–Berry models and their sensitivity of stomatal conductance to environmental changes. The Noah land model is based on coupling the diurnally dependent Penman potential evaporation approach with the multilayer soil model of Mahrt and Pan (1984). In the Noah land model, the total evaporation E is the sum of 1) direct evaporation from the surface E_{dir}, 2) evaporation from precipitation intercepted by the canopy E_c, and 3) canopy

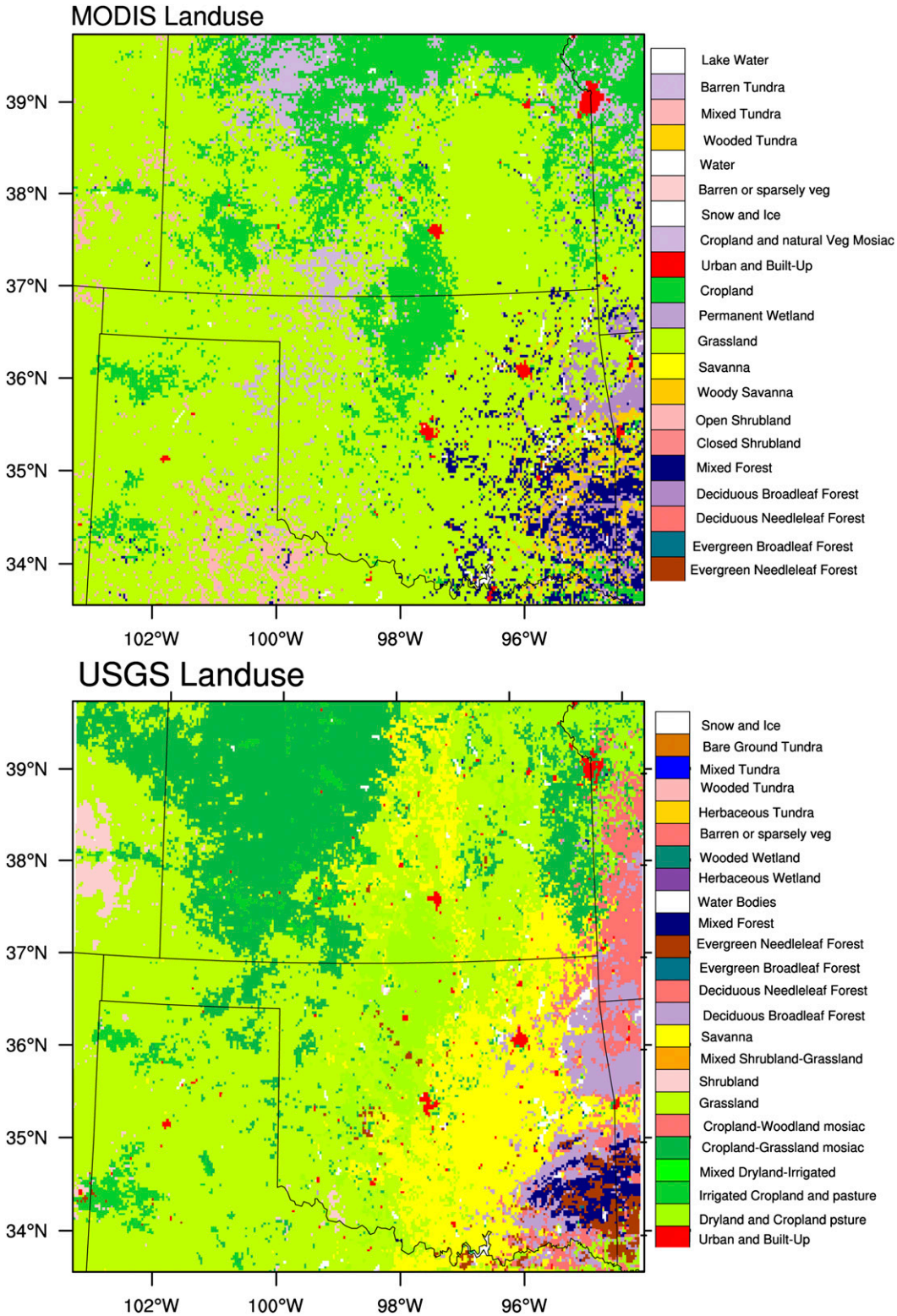

FIG. 1. Land-use map from (top) MODIS and (bottom) USGS.

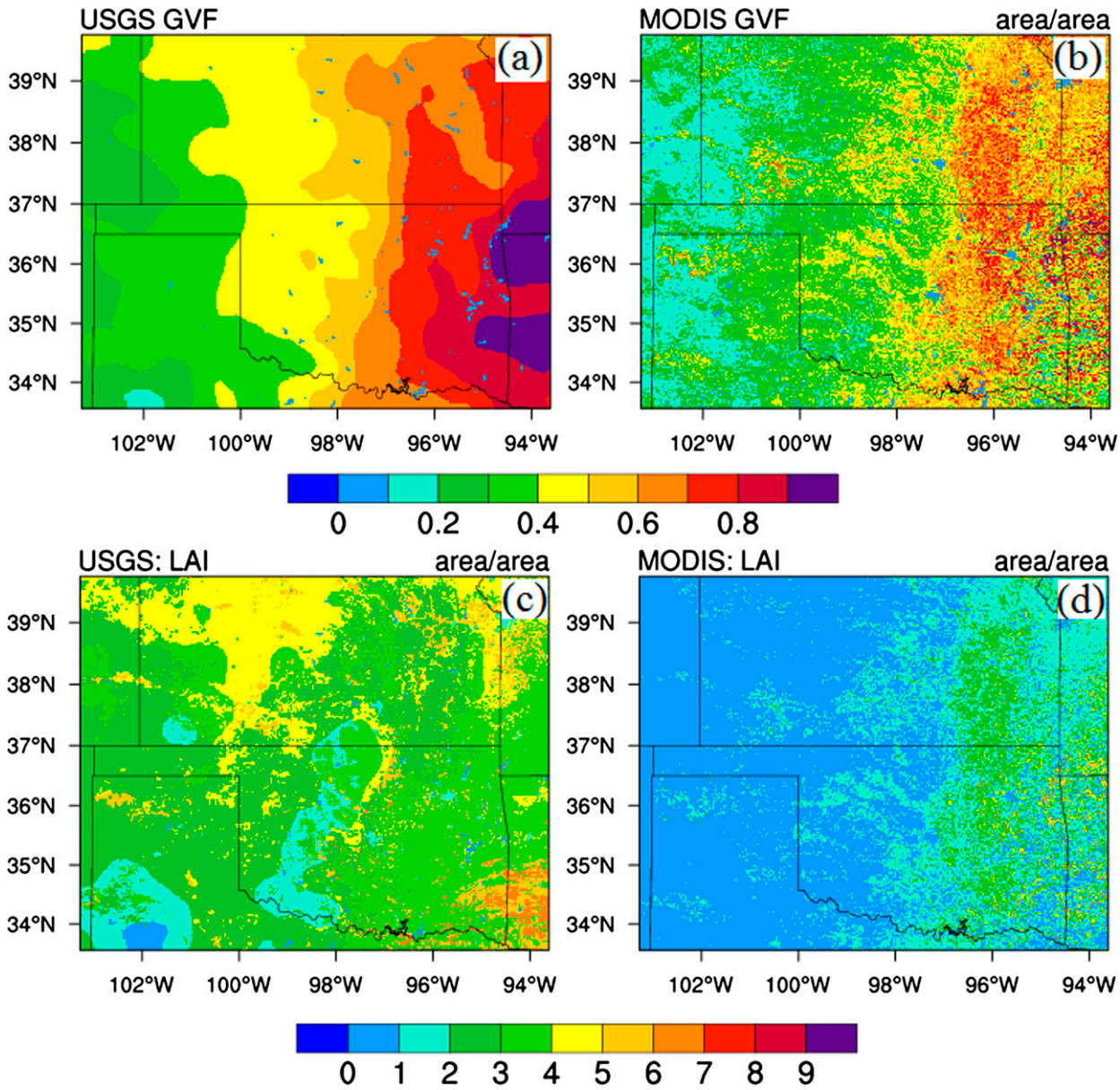

FIG. 2. (left) USGS and (right) MODIS values, showing differences in (a),(b) GVF and (c),(d) LAI maps.

evapotranspiration E_t. The total evaporation E is thus given as

$$E = E_{\mathrm{dir}} + E_c + E_t. \tag{1}$$

The E_t variable includes the R_c term in the following way:

$$E_t = \sigma_f E_p B_c \left[1 - \left(\frac{W_c}{S}\right)^n\right], \tag{2}$$

where σ_f is the green vegetation fraction and is responsible for differentiating the total evaporation into soil direct evaporation and canopy transpiration, E_p is potential evaporation, W_c is intercepted canopy water content, S is the maximum canopy capacity (value used here is 0.5), and n is 0.5; B_c is a function of canopy resistance and is formulated as

$$B_c = \frac{1 + \dfrac{\Delta}{R_r}}{1 + R_c C_h + \dfrac{\Delta}{R_r}}, \tag{3}$$

where Δ and R_r are dimensionless terms, C_h is the surface exchange coefficient for heat and moisture, and R_c

is the canopy resistance. The details of all parameters are available in Ek and Mahrt (1991). The canopy-resistance approach of Noilhan and Planton (1989) and Jacquemin and Noilhan (1990) is implemented within the Noah LSM framework by Chen et al. (1996) and Chen and Dudhia (2001a).

Niyogi et al. (2009) highlight the different reasons for adopting photosynthesis-based schemes rather than a Jarvis-type approach within an NWP framework. These primarily include the dependence of the Jarvis approach on the significantly uncertain prescription of minimum stomatal resistance $R_{c,\min}$ (Niyogi and Raman 1997; Alfieri et al. 2008), which generally varies from vegetation to vegetation and should not be treated as a constant.

The photosynthesis parameterization, however, is complicated and requires iterative solutions, and hence an outstanding question is whether the photosynthesis-based approach should be adopted in NWP. Therefore, assessment of new satellite data and calibration of the $R_{c,\min}$ term were conducted to determine if it significantly enhanced the performance of the current Jarvis-type R_c model in the Noah LSM. As stated, this question has become urgent in light of experiments at NCEP that showed systematic improvements in NMM and GFS can be achieved by modulating the $R_{c,\min}$ term (Mitchell 2005; Alfieri et al. 2008; Ronda et al. 2001).

The Jarvis scheme is based on Jacquemin and Noilhan (1990) and estimates R_c from the following formulation:

$$R_c = \frac{R_{c,\min}}{\mathrm{LAI} \times \mathrm{F1} \times \mathrm{F2} \times \mathrm{F3} \times \mathrm{F4}}, \tag{4}$$

where F1, F2, F3, and F4 are environmental stress functions. The stress function values range from 0.05 to 1 and represent the effects of solar radiation, humidity, air temperature T_a, and soil water availability, respectively, on R_c. All of the stress functions are crucial parameters describing the interaction between plant and environment in the presence of radiation and humidity. One form of the stress function representation is given as

$$\mathrm{F1} = \frac{R_{c\min}/R_{c\max} + f}{1 + f}, \quad \text{where} \quad f = 0.55\frac{R_g}{R_{gl}}\frac{2}{\mathrm{LAI}}, \tag{5}$$

$$\mathrm{F2} = \frac{1}{1 + \mathrm{VPD}[q_s(T_a) - q_a]}, \tag{6}$$

$$\mathrm{F3} = 1 - 0.0016(T_{\mathrm{ref}} - T_a)^2, \quad \text{and} \tag{7}$$

$$\mathrm{F4} = \sum_{i=1}^{3} \frac{(\Theta_i - \Theta_w)d_z}{(\Theta_{\mathrm{ref}} - \Theta_w)(d_{z1} - d_{z2})}. \tag{8}$$

In these equations, R_{gl} is the radiation lower limit for photosynthesis/transpiration to be initiated, R_g is the surface global radiation, VPD is the vapor pressure deficit, and Θ_{ref} and Θ_w are the field capacity and wilting point, respectively. Furthermore, $R_{c\max}$ is the cuticular resistance of leaves, which is set to 5000 s m^{-1}, and T_{ref} is the reference temperature for the leaf to transpire, which is set to 298 K. Also, $q_s(T_a)$ is the saturated water vapor mixing ratio at T_a, q_a is water mixing ratio, and d_z is the soil depth thickness. More details are provided in Chen and Dudhia (2001a).

One representation of the photosynthesis-based canopy-resistance scheme can be written as (Ball et al. 1987)

$$\frac{1}{R_s} = g_s = m\frac{A_n h_s}{C_s} + b \quad \text{and} \tag{9}$$

$$R_c = R_s/\mathrm{LAI},$$

where R_s is the stomatal resistance, g_s is the stomatal conductance term, and R_c is the canopy resistance. Other variables include the photosynthesis rate A_n, relative humidity at the leaf surface h_s, and CO_2 concentration at the leaf surface C_s. The terms m and b are linear expressions that are based on gas-exchange measurements (Ball et al. 1987) and are predominantly a function of the vegetation type and the photosynthesis pathway (Sellers et al. 1996b; Niyogi et al. 2009; Ball et al. 1987). In GEM, A_n is obtained using the Ball–Berry model [Eq. (9)] with the Collatz et al. (1991, 1992) scheme. The coupling between h_s and C_s follows the Sellers et al. (1996a) approach.

Thus, the difference in these two stomatal resistance approaches is that the Jarvis stomatal resistance model depends on meteorological parameters such as light, temperature, humidity, and soil moisture conditions. The Jarvis model assumes that stomatal resistance is a multiplicative function of the environmental stress terms applied to the landscape-dependent "minimum stomatal resistance" term. The Jarvis scheme does not consider carbon dioxide and explicit estimates of leaf temperature or transpiration. In other words, the Jarvis scheme works well as a canopy-resistance model requiring only those variables as input that are typically available from a meteorological model. On the other hand, the Ball–Berry scheme has several appealing attributes such as its ability to capture ecophysiological and biogeochemical factors such as leaf photosynthetic capacity and ambient CO_2. More relevant to meteorological applications is that the Ball–Berry scheme appears to be better suited for a range of environmental conditions and requires fewer tuning parameters than does the Jarvis scheme. Additional benefits of using the Ball–Berry scheme over the Jarvis approach are discussed in Niyogi et al. (2009).

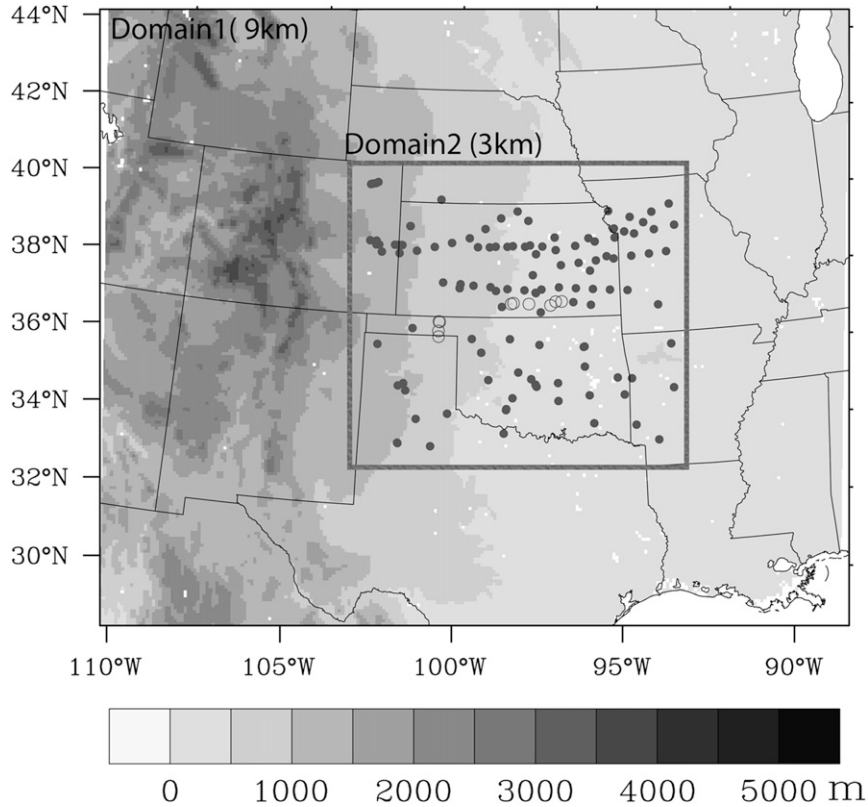

FIG. 3. Model domain and elevation map. Ten IHOP_2002 field data sites are marked with an open circle, and 71 NWS station data locations are marked with small dots.

In section 4, modifications to the existing WRF model are considered.

4. WRF model description and domain configuration

The WRF model is a primitive-equation, nonhydrostatic, compressible model. The model has domain-nesting capabilities, which allow finer spatial resolution over areas of interest. This model is widely used in many countries for the operational purposes of weather prediction. The simulations in this paper were carried out with the Advanced Research configuration of the WRF model, version V3.0.1 (Skamarock et al. 2005). The model boundary and initial conditions of large-scale atmospheric fields, soil parameters (moisture and temperature), and sea surface temperature were given by the 1°, 6-hourly NCEP Global Final Analysis (FNL) data available online (http://dss.ucar.edu/datasets/ds083.2/). FNL data were chosen because they are commonly used forcing data for regional weather prediction and are a reference to this study because other regions such as Asia and Africa still depend on NCEP FNL 1° forcing data. These forcing data were interpolated to the respective WRF grid using the WPS (http://www.mmm.ucar.edu/wrf/users/wpsv3/wps.html). For this study, two nested domains were configured as shown in Fig. 3. Domain 1 is the coarsest mesh and has 237 × 201 grid points in the north–south and east–west directions, respectively, with a horizontal grid spacing of 9 km. Within domain 1, domain 2 is nested with 280 × 229 grid points at 3-km grid spacing. Domains 1 and 2 run together with a two-way nested interaction. The topographic features at 9-km resolution, with high elevation in the west and low elevation in the east, are shown in Fig. 3. The model's 28 vertical layers use terrain-tracking coordinates from the surface to the 10-hPa pressure level.

The model simulations were conducted using the following physics-based options: the WRF single-moment six-class (WSM6) bulk microphysical parameterization scheme (Hong et al. 2004; Hong and Lim 2006), the Betts–Miller–Janjić cumulus parameterization scheme that is based on the Betts–Miller convective adjustment scheme (Betts 1986; Betts and Miller 1986), the Yonsei University planetary boundary layer scheme of Hong and Pan (1996), the Noah land surface model (Chen and Dudhia 2001a; Ek et al. 2003), the Rapid Radiative Transfer Model (Mlawer et al. 1997) for

TABLE 1. WRF-based six-experiment design using USGS and MODIS in various combinations of land use, LAI, and GVF.

Expt	Model	Canopy-resistance scheme	Land-use map	LAI	GVF
EXPT-1	WRF	Jarvis	USGS	Table LAI	Default
EXPT-2	WRF	Jarvis	MODIS	Table LAI	Default
EXPT-3	WRF	Jarvis	MODIS	MODIS	MODIS
EXPT-4	WRF_GEM	Ball–Berry	USGS	Table LAI	Default
EXPT-5	WRF_GEM	Ball–Berry	MODIS	Table LAI	MODIS
EXPT-6	WRF_GEM	Ball–Berry	MODIS	MODIS	MODIS

longwave radiation calculations, and the shortwave radiation calculation that is based on Dudhia (1989).

5. Experimental design and data

A set of six coupled model experiments was conducted using WRF for a severe convective thunderstorm episode over the southern Great Plains that occurred during the International H_2O Project (IHOP_2002; 28–31 May 2002) field experiments. The 9-km-resolution domain was used to cover more observed station data and for verification. The six-member ensemble experiments are described in Table 1. All six experiments were conducted using some combination of 1) USGS or MODIS land-use categories, 2) lookup-table LAI or MODIS LAI values, 3) MODIS GVF or climatological GVF, or 4) default WRF–Noah with the Jarvis canopy-resistance scheme or the WRF–Noah–GEM with a photosynthesis-based canopy-resistance scheme. For all of these experiments (Table 1), an attempt was made to evaluate in a more quantitative way the impact of new, remotely sensed surface data working in conjunction with the two canopy-resistance formulations.

Two sources of observational field-experiment and station data were used for model verification. The first, IHOP_2002, was a field experiment that took place over the SGP from 13 May to 25 June 2002 (Weckwerth et al. 2004) that consisted of 10 sparsely located surface flux sites across the SGP region (open circles marked in Fig. 3). These sites measured surface parameters (surface turbulent fluxes, soil temperature and moisture, etc.; LeMone et al. 2007) over different vegetation types. For the second source, the U.S. Department of Energy (DOE) Atmospheric Radiation Measurement Program (ARM)/AmeriFlux network of data stations (FLUXNET) was also used (marked with a star in Fig. 3). In addition to meteorological information, these stations collected data on landscape and plant canopy/biophysics, soil characteristics and soil variables, and surface hydrological behavior. These data allowed us to validate the impact of remotely sensed data over USGS-obtained land data (i.e., LAI, GVF, and land use) along with two canopy-resistance schemes in the model over the three AmeriFlux data stations. All of these stations (Walnut, Kansas; Bondville, Illinois; and Niwot, Colorado) consisted of different vegetation, soil, and surface conditions.

6. Analysis

All simulations were conducted for the period spanning 28–31 May 2002 (4-day simulation) and were verified for 30 May 2002. To quantify a clear impact via new land-use and remote sensing data, the third day of simulation data was used (30 May 2002) for analysis because it was a clear-sky day with no reported storms across the SGP region. Another advantage of using the third day of simulations was that after 48 h of model simulation the model-estimated surface flux and other meteorological parameters were more sensitive to LAI (Charusombat et al. 2010; Rosero et al. 2010). With proper model spinup, the effect of these parameters can be more appropriately studied. Six sets of experiments were conducted for this period. These experiments were limited largely by computational constraints, and hence our study was limited to only one summer case.

To summarize the weather conditions for 28–31 May 2002, a synoptic analysis suggested that a closed, upper-level low was positioned over western Oklahoma at 1200 UTC 28 May 2002 and slowly drifted eastward during the day, ultimately staying west of Oklahoma through the late afternoon and producing a few thundershowers. On 29 May, clear skies were seen, with an upper-level high located over Colorado. Southerly winds measuring 40 m s^{-1} at 300 hPa were found over Colorado while a weak, upper-layer trough was observed over eastern Oklahoma. On 30 May, there was a north–south line of rain showers at the dryline in the eastern Texas Panhandle with light southerly winds. Clear skies were observed on 31 May 2002 over the southern Great Plains region.

a. Surface heat fluxes and soil temperature differences

All six experiments showed only small differences in spatial pattern across the domain for both latent and sensible heat fluxes. Differences in magnitude were found, however, which was expected since changes in land use/cover and newly input remotely sensed data

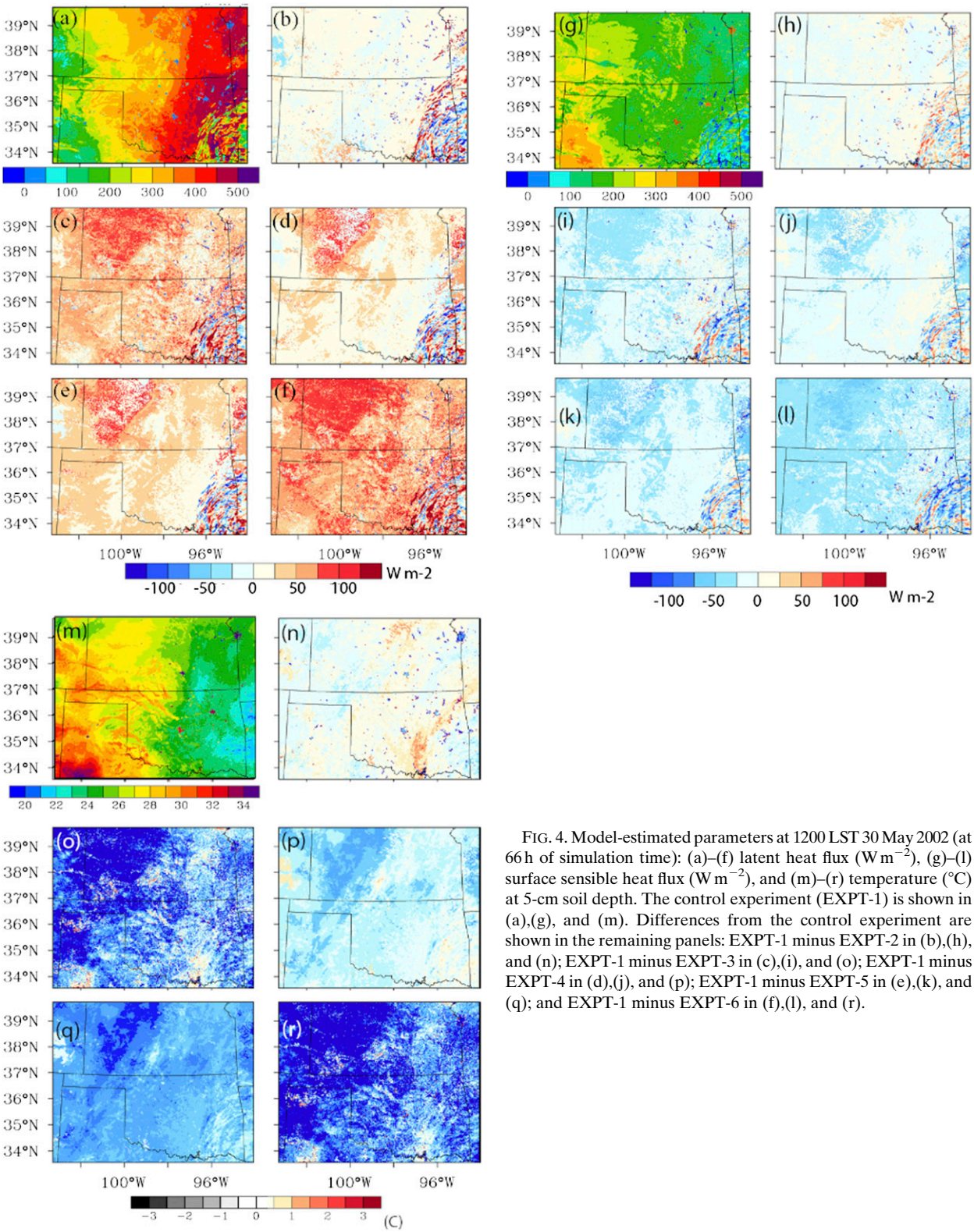

FIG. 4. Model-estimated parameters at 1200 LST 30 May 2002 (at 66 h of simulation time): (a)–(f) latent heat flux ($W\,m^{-2}$), (g)–(l) surface sensible heat flux ($W\,m^{-2}$), and (m)–(r) temperature (°C) at 5-cm soil depth. The control experiment (EXPT-1) is shown in (a),(g), and (m). Differences from the control experiment are shown in the remaining panels: EXPT-1 minus EXPT-2 in (b),(h), and (n); EXPT-1 minus EXPT-3 in (c),(i), and (o); EXPT-1 minus EXPT-4 in (d),(j), and (p); EXPT-1 minus EXPT-5 in (e),(k), and (q); and EXPT-1 minus EXPT-6 in (f),(l), and (r).

were added. Figures 4a–f and 4g–l show the spatial distribution of the simulated noontime latent and sensible heat fluxes, respectively, on 30 May 2002. On a spatial scale, some differences in latent and sensible fluxes are clearly noted in all six experiments. The first two experiments (EXPT-1 and EXPT-2; Fig. 4b) show very similar results in both spatial patterns and magnitude but do show minor differences. For noontime domain-averaged latent heat fluxes, EXPT-1, conducted using default Noah settings in the WRF model, shows 321 $W m^{-2}$ whereas EXPT-2, conducted with similar settings but instead using MODIS land-use data, gives values of 313 $W m^{-2}$. This result suggests that if more recent MODIS land-use maps are used the model then shows slightly less latent heat flux ($\sim$10 $W m^{-2}$). This difference is mainly because much of the cropland is changed to grassland in MODIS land-use data and therefore evapotranspiration of cropland is changed to evapotranspiration of grassland. An additional objective is to assess the impact of canopy resistance; therefore, two experiments have identical settings except that their canopy-resistance schemes are different. These two experiments (EXPT-3 and EXPT-6) are conducted with MODIS input data (land use, LAI, and GVF), and it is clear that the Noah–GEM scheme produces less latent heat flux than the Jarvis scheme does: the domain-averaged analysis suggests that the Noah–GEM scheme produces $\sim$30 $W m^{-2}$ less latent heat flux than the Jarvis scheme does. Further, the Noah–GEM scheme is used with USGS and MODIS land-use input data, and comparison suggests that the Noah–GEM scheme with MODIS data produces slightly less latent heat flux than does the Noah–GEM scheme using USGS land-use data. Overall, these experiments exhibit some differences in their outcome. The results from experiments EXPT2–EXPT6 are separated from the control experiment (EXPT1) and indicate that the surface heat fluxes differences are large when the Noah–GEM scheme is used with MODIS-sensed parameters. The latent heat flux is evaluated over station data with station-measured fluxes in a later section, but with spatial-patterns analysis there is some degree of difference in surface heat flux. A similar but opposite response is seen in the sensible heat flux and is shown in Figs. 4g–l. The MODIS land-use experiments are 28 $W m^{-2}$ warmer than the USGS land-use map experiments, whereas the Noah–GEM scheme responses are only slightly warmer than the response from the Noah–Jarvis scheme (Fig. 4l). The largest change in the magnitude of temperature or any other associated parameter was seen over Nebraska and Oklahoma, mainly due to large land-use differences between the USGS and MODIS datasets. The effect on savanna vegetation appeared to be more significant in Oklahoma since it was transformed into grass and croplands when the MODIS land-use map was involved. Another region that saw a significant impact was Nebraska. The crop and savanna areas, as defined by USGS, were converted to large-scale grasslands in the MODIS product. In later sections we investigate these results more quantitatively.

The simulations that included the MODIS-based land-use map and the MODIS GVF parameter showed large differences between the Noah–Jarvis and Noah–GEM R_c schemes, especially for air temperature patterns over Oklahoma. Through EXPT-3 and EXPT-6, we found that Noah–GEM projected 2°–3°C higher than Noah–Jarvis (not shown) and has a lower mixing ratio and less latent heat flux (Figs. 4a–f) than the Noah–Jarvis model. The simulated latent heat fluxes from all experiments show some interesting points: 1) the Noah–Jarvis scheme produces higher latent heat fluxes than Noah–GEM, 2) better representation of latent heat flux is noted with MODIS land-use input data, and 3) with more realistic MODIS land-use input the model is able to capture distinctness in latent heat flux patterns associated with different vegetation types.

Soil temperature is another important parameter obtained from the remotely sensed datasets and is directly related to surface properties such as vegetation type. The vegetation fraction and soil surface/skin temperature show a high degree of interdependence (Mostovoy et al. 2008). Therefore, we expected the model-predicted soil temperature to follow the vegetation indices. Figures 4m–r show simulated soil temperature (5-cm soil depth) from the six sets of experiments. Minor differences were noted between the simulated soil temperature of the USGS-based land-use simulation (EXPT-1) and the MODIS-based simulation (EXPT-2). Soil temperature patterns that closely followed the MODIS-based vegetation-map pattern (Figs. 4o,r) were noted. The east side of the domain consisted of tall vegetation while the west side of the domain showed grasslands (Fig. 1). Therefore, a lower soil temperature over the tall vegetation and a higher soil temperature from both short vegetation types and bare surfaces were expected. Similar results were found from the Noah–GEM scheme when used in conjunction with MODIS input data (EXPT-6). The analysis concluded that the differences in soil temperature in the MODIS land-use map were only significant when MODIS-based GVF and LAI were used (Figs. 4o,r) and after coupling MODIS input data with the Noah–GEM model. Figures 4o and 4r show that soil temperature followed the MODIS-sensed vegetation indices well.

The verification statistics for 2-m air temperature and 2-m mixing ratios are shown in Table 2. The verification was based on domain-averaged analysis and used National Weather Service (NWS) surface observations

TABLE 2. Domain-averaged bias and RMSE at 1200 LST 30 May 2002 (at 66 model forecast hours). NWS surface observations from 71 sites across simulation domain 2 (at 3-km resolution) were used to calculate the average errors in temperature and mixing ratio. Here, CI indicates confidence interval.

Expt	Temperature bias (K) with 95% CI	Temperature RMSE (K)	Mixing ratio bias ($g\,kg^{-1}$) with 95% CI	Mixing ratio RMSE ($g\,kg^{-1}$)
EXPT-1	−0.38	1.23	−1.34	2.05
EXPT-2	−0.68	1.28	−1.13	2.05
EXPT-3	−0.04	1.20	−1.53	2.32
EXPT-4	−0.32	1.24	−1.92	2.62
EXPT-5	0.14	1.28	−1.84	2.54
EXPT-6	1.56	2.01	−2.60	3.13

from 71 sites across the model domain (inner domain at 3-km resolution) to calculate average errors of temperature and mixing ratio. From Table 2, EXPT-3 had the best results of all six sets of experiments and showed less bias and RMSE in air temperature but also reproduced a slightly higher mixing ratio. The small bias in air temperature was found in those experiments that were performed using USGS land-use information. This result may be due to the tuning that has been done on the different model parameters for this region (LeMone et al. 2008). The domain-averaged bias and RMSE in air temperature and mixing ratio suggested that there was much improvement in surface temperature and mixing ratio after using MODIS land-use data and the input of MODIS-based LAI and GVF products. Of interest is that the coupled Noah–GEM (EXPT-6) with MODIS data input resulted in large biases and RMSE in air temperature (Table 2). The domain-averaged analysis provides limited information to determine the capabilities of the Noah–GEM canopy scheme for this case-study analysis. Therefore, to explore further the impact of MODIS input data along with two-canopy resistance, the following section outlines the analysis over individual station data where different vegetation types were present.

b. *Verification over IHOP_2002 data sites*

Surface-measured data over 10 observation sites from the IHOP_2002 field campaign were used as well as documentation about each location and its environmental conditions, as provided in LeMone et al. (2007) and Alfieri et al. (2009). The chosen sites were located across the SGP region. LeMone et al. (2008) also investigated the impact of surface heterogeneity on 28 May 2002, a clear-sky day, using an offline Noah LSM (uncoupled from an atmospheric modeling system). In this section, we evaluated our coupled-model experiments (Table 1) against the 10 IHOP_2002 data sites for evaluation.

To evaluate the surface flux partitioning and other surface meteorological parameters such as mixing ratio, 2-m air temperature, and 10-m east–west U and north–south V wind components in all six unique experiments, we conducted an additional analysis for each of the individual days (28–30 May 2002). Daytime-averaged data [1000–1500 local standard time (LST)] that were averaged again over the 10 IHOP_2002 sites for 28–30 May 2002 are shown in Fig. 5. Figures 5a and 5b show latent and sensible heat fluxes and provide the performance of each respective experiment by their position between the lower- and upper-bound values. The latent heat flux simulated in EXPT-1 (from USGS land-use input) is higher than that for EXPT-2 (MODIS land-use input) on all three days (Fig. 5a). The latent heat flux from the MODIS-input-data experiments performed with Noah–Jarvis (EXPT-3) showed projections that were close to the observed mean value. The latent heat flux from the Noah–GEM scheme combined with the MODIS input data (EXPT-5 and EXPT-6) gave values that were lower than the observational average. In a similar way, sensible heat is presented in Fig. 5b and shows all experiments that fall into the upper, high limit of observed sensible heat flux on all three days. The 29 May clear-sky case offered good documentation of both surface and environment conditions (LeMone et al. 2008). The experiment (EXPT-6) that is based on the Noah–GEM scheme with MODIS input data showed a mean sensible heat flux value that was even higher than the upper limit of the observed sensible heat flux. When compared with observed surface flux data, the analysis suggests that EXPT-3 (Noah–Jarvis with MODIS input data) is in good agreement with all experiments but still left a larger question concerning balancing the latent and sensible heat fluxes. To address this shortcoming, an energy-balance analysis between Noah–Jarvis and Noah–GEM was performed to determine why Noah–GEM was unable to balance the latent and sensible heat fluxes simultaneously. First, the downward shortwave radiation was compared and was found to be in good agreement with observed data. Second, the modeled soil heat flux was checked and was compared with the observed soil heat flux using IHOP_2002 data sites. The observed soil heat flux was found to reach down to $-200\,W\,m^{-2}$ while the model reproduced about $-150\,W\,m^{-2}$ of soil heat flux in both the Noah–Jarvis and Noah–GEM models. This partitioning is important since surface energy balance is dependent upon soil condition and surface vegetation, both of which provide a key link between the atmosphere and the water/energy balances at the earth's surface (Wei 1995; Robock et al. 2000; Leese et al. 2001). Even though a more detailed surface canopy-resistance scheme was introduced within

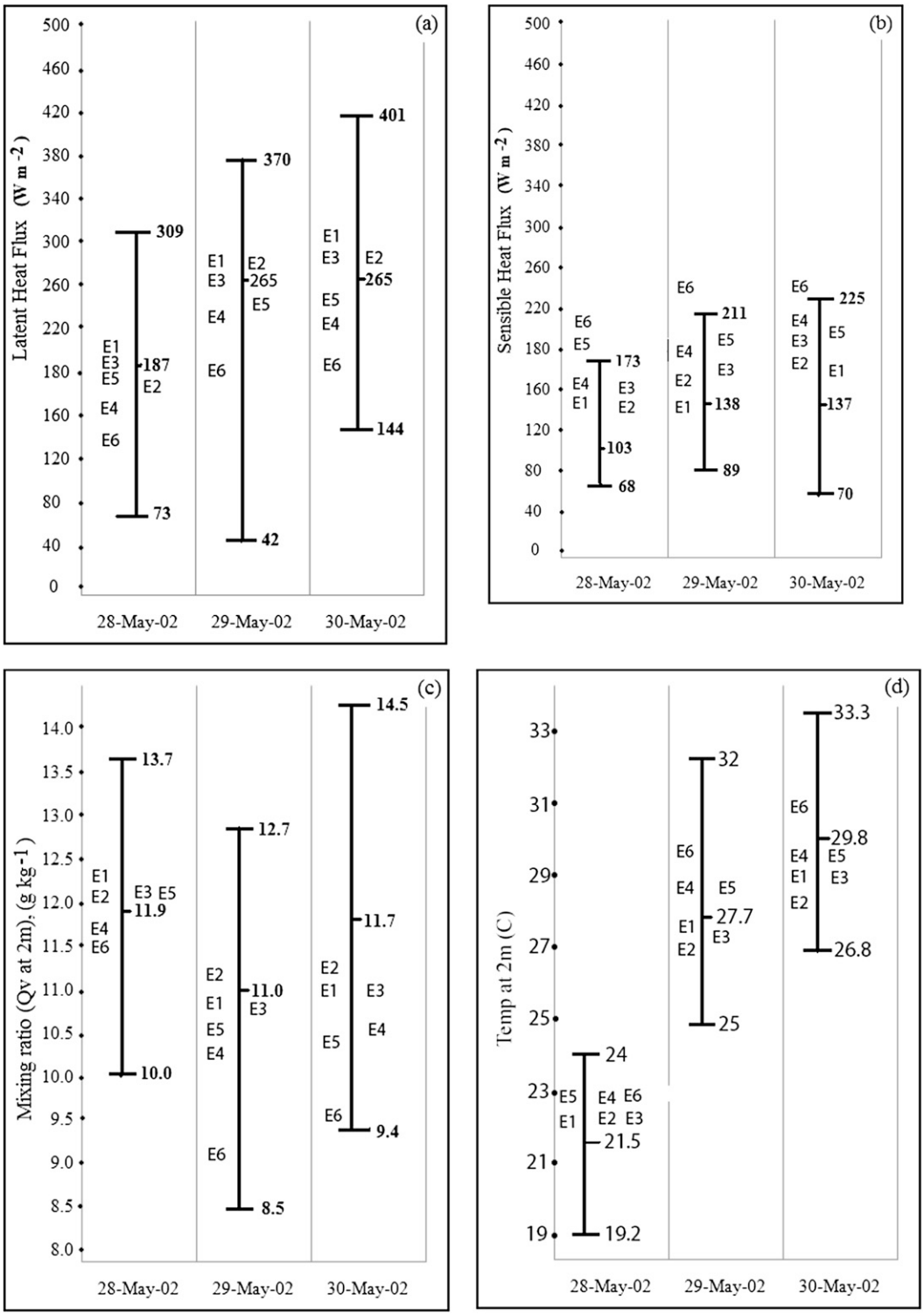

FIG. 5. Daytime model results and observations averaged between 1000 and 1500 LST and averaged over 10 IHOP_2002 data sites for 28–30 May 2002. The thick vertical lines correspond to the range of surface observational data between 1000 and 1500 LST. The horizontal bars indicate the lower and upper limits to the observations, with the averaged value for the hourly observed data during that period marked between those limits. E1–E6 are the results for the model experiments listed in Table 1. Shown are (a) surface latent heat flux ($W\,m^{-2}$), (b) surface sensible heat flux ($W\,m^{-2}$), (c) 2-m surface mixing ratio ($g\,kg^{-1}$), and (d) 2-m air temperature (°C).

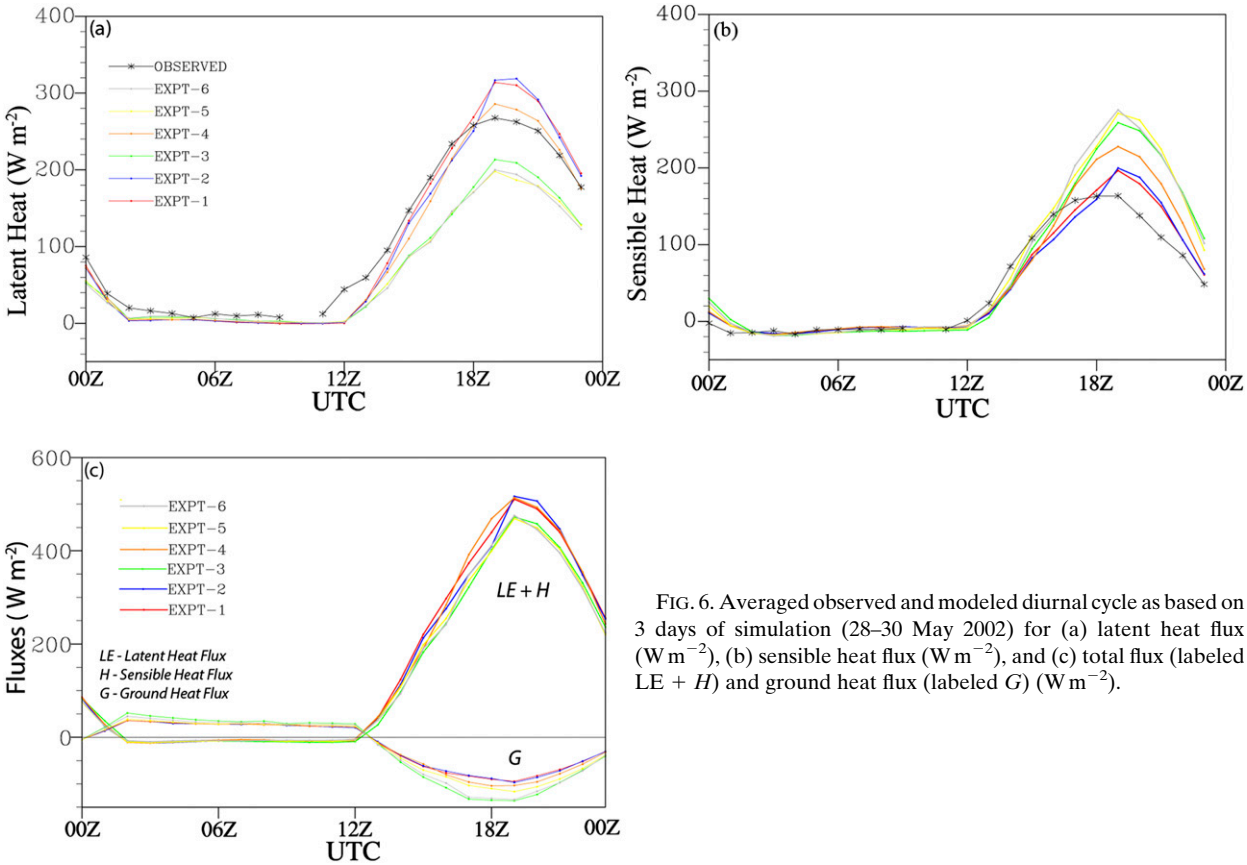

FIG. 6. Averaged observed and modeled diurnal cycle as based on 3 days of simulation (28–30 May 2002) for (a) latent heat flux ($W\,m^{-2}$), (b) sensible heat flux ($W\,m^{-2}$), and (c) total flux (labeled LE + H) and ground heat flux (labeled G) ($W\,m^{-2}$).

the Noah land surface model, it did not improve the energy flux partitioning. As it stands, there is a need to test such a scheme more closely so as to optimize input parameters (LAI, roughness length, $R_{c,\min}$, and Zilitinkevich coefficient) within the Noah land surface model and the GEM model (especially the Vmax input in GEM), which might have caused such feedback over different geographical locales.

The mixing ratio and 2-m air temperature analyses are shown in Figs. 5c and 5d. Here, the mixing ratio and 2-m air temperature improved after the model was configured with MODIS data (EXPT-3). The Noah–GEM coupled model experiments (EXPT-4, EXPT-5, and EXPT-6) placed the mixing ratio in the lower range of the observed values (i.e., below the mean observed value), whereas the air temperature was found to be in the upper range shown in Fig. 5d. The averaged U component of the 10-m wind for 28 May was below the mean observed value from all six experiments (not shown). The experiments for the rest of the days all showed mixed results close to the average wind value, however. Similar results were found for the V wind component (not shown). Differences in 10-m winds were small among the experiments, but the MODIS-input-data experiment (EXPT-3) showed a much closer match as based on all 3-day analyses when compared with observed data.

The 3-day diurnal-averaged cycle for surface heat fluxes and ground heat fluxes is shown in Figs. 6a–c. From Fig. 6a, The experiments that are based on Noah–Jarvis with default input parameters (LAI, GVF, and land use) show higher latent heat fluxes than does Noah–GEM. The experiments that are based on MODIS GVF (EXPT-3, EXPT-5, and EXPT-6) show lower latent heat flux and higher sensible heat flux. The observed latent and sensible heat fluxes do not match with any experiments; that is, almost all experiments overestimate the sensible heat fluxes. We also analyzed the model-resolved energy balance between total flux (latent + sensible) and ground heat flux (Fig. 6c), however, and found that the Noah–GEM reproduces less total flux, which in turn leads to more energy stored as a ground heat flux (Fig. 6c). None of the experiments show correct energy balance in the land surface model, which poses a broader question about the distribution of energy balance in the model and shows a need for a future study that involves better representation of canopy- and leaf-based energy flux estimation within the model.

TABLE 3. Impact on boundary layer, as based on domain-averaged analysis and the average from the surface to the 700-hPa level (1025-, 975-, 950-, 925-, 900-, 875-, 850-, 825-, 800-, 775-, 750-, and 700-hPa levels). Bias and RMSE are at 1800 LST (0000 UTC) 30 May 2002 (at 48 model forecast hours) from the NWS surface with upper-air sounding observations from 71 sites across model domain 2 (at 3-km resolution).

	Temperature (K)		Mixing ratio ($g\,kg^{-1}$)		Wind speed ($m\,s^{-1}$)		Relative humidity (%)	
Expt	Bias	RMSE	Bias	RMSE	Bias	RMSE	Bias	RMSE
EXPT-1	0.388	1.291	0.981	2.108	1.938	5.213	6.626	17.45
EXPT-2	0.252	1.268	0.942	2.008	1.888	5.180	6.351	16.73
EXPT-3	0.464	1.367	0.638	2.053	1.615	5.203	4.561	16.65
EXPT-4	0.704	1.499	0.482	2.176	1.431	5.161	3.292	17.06
EXPT-5	0.671	1.356	0.844	2.074	1.530	5.195	5.071	16.25
EXPT-6	1.314	1.345	0.588	2.655	1.227	4.882	4.018	20.01

These findings again suggest that the default NOAH land surface model in the WRF modeling framework when using MODIS land use, MODIS GVF, and MODIS LAI gives the best results among the different experiments. Second, Noah–Jarvis also provided good results for both surface fluxes and mixing ratio when used in conjunction with MODIS land use, MODIS GVF, and MODIS LAI. On 28 May, simulated sensible heat flux was much higher than the averaged observed values of 29 and 30 May. Almost all of the six experiments simulated the sensible flux in the upper range of the observed sensible heat flux and, thus, suggested that surface energy flux partitioning was not balanced correctly within the Noah land surface model used in WRF.

c. *Impact on boundary layer moisture, temperature, wind speed, and relative humidity*

Surface and boundary layer processes determine how much heat and water are exchanged between the surface and the boundary layer and between the boundary layer and the free atmosphere. Therefore, we investigated the impact of the six experiments to quantify the impact of temperature, moisture, wind speed, and relative humidity in the boundary layer. To do this, we conducted a quantitative analysis in terms of bias and RMSE for temperature, mixing ratio, wind speed, and relative humidity. First, the model domain averages (bias and RMSE) were analyzed using NWS-based upper-air sounding profiles for areas across the model domain. After that, the data found over the layers that fall between the surface and the 700-hPa atmosphere height, which covers the boundary layer, were averaged (1025, 950, 925, 850, 825, 800, 775, 750, and 700 hPa). The bias and RMSE were calculated for 0000 UTC (1800 LST) and 1200 UTC (0600 LST) on 30 May 2002 because these times coincide with the observation schedule of the upper-air sounding measurements. Table 3 shows the bias and RMSE at 1800 LST on 29 May, whereas Table 4 shows the data analysis from 0600 LST on 30 May. Experiments listed in Table 3, such as EXPT-3 and EXPT-6, which are designed to use MODIS products, show a slightly higher bias/RMSE for temperature but a lower bias/RMSE for mixing ratio, wind speed, and relative humidity in the boundary layer. EXPT-3 used the Noah–Jarvis scheme, and EXPT-6 used the Noah–GEM scheme along with MODIS data, and both obtained a better response in mixing ratio and relative humidity. Still, mixed results were obtained from all experiments for the 0600 LST analysis (Table 4). The simulation of the early morning and the nocturnal boundary layer is a broader challenge (Shin et al. 2012), and hence results make it difficult to determine which experiment gave the best results. Some MODIS-based experiments (EXPT-3) showed less bias in wind speed or mixing ratio. The precipitation amount is the helpful measure of any numerical model simulation; therefore, precipitation analyses were conducted by averaging total precipitation over the model's inner domain and comparing the results with stage-IV observed precipitation averaged over the same domain area. EXPT-3, which is conducted with MODIS input data using the Noah–Jarvis scheme, was in close agreement with observed precipitation (Table 5). Of interest is that all experiments overestimated precipitation and that precipitation was improved by the input of MODIS land surface data.

Our bias and RMSE statistics of the boundary layer suggest that, in comparison with all other experimental model designs, model-simulated results improved with MODIS data working together with the default Noah. Conversely, adopting Noah–GEM, when integrated with MODIS data, did improve results for mixing ratio, wind speed, and relative humidity but gave a slight bias in temperature within the boundary layer. Therefore, this analysis concludes that the MODIS data show first-order improvement in the simulation of thermodynamic and dynamic features within the ABL.

TABLE 4. As in Table 3, but conducted at 0600 LST (1200 UTC) 30 May 2002 (at 60 model forecast hours).

	Temperature (K)		Mixing ratio ($g\,kg^{-1}$)		Wind speed ($m\,s^{-1}$)		Relative humidity (%)	
Expt	Bias	RMSE	Bias	RMSE	Bias	RMSE	Bias	RMSE
EXPT-1	0.033	1.549	0.772	2.293	2.014	5.074	3.265	17.89
EXPT-2	−0.087	1.604	0.740	2.342	2.333	5.256	3.571	18.95
EXPT-3	0.005	1.483	0.754	2.155	2.222	5.481	2.350	16.00
EXPT-4	0.197	1.556	0.783	2.193	2.095	5.391	2.661	17.30
EXPT-5	0.189	1.376	0.437	2.028	1.830	5.021	2.380	16.71
EXPT-6	0.544	1.509	0.376	2.020	2.377	5.215	0.346	17.39

7. Conclusions and discussion

There has been a great deal of effort focused on improving the different parameterization schemes by means of integrating high-model-resolution products into the current state of any given weather model that is widely used for short-term weather forecasting (Case et al. 2011). The current surface parameterizations used in land surface models lack the vital information of the complex, real-time surface exchange processes affecting weather predictions, however. A data-integration and modeling study was conducted that was aimed at using remotely sensed vegetation characteristics to better characterize the vegetation input parameter. Overall, the results led to the following conclusions.

1) There were significant differences between the new MODIS land-use map and the previous USGS land-use map across the model domain. First, where the savanna vegetation type was prominent in the USGS-based land-use map it is not present in the new MODIS-based land-use map and deciduous broadleaf forests and deciduous needle-leaf forests were less prominent in the newer MODIS land-use data. In addition, cropland was categorized into grassland over western Nebraska and some northern areas of Oklahoma. Second, real-time LAI and GVF from the new MODIS data were used, and this method led to different values than were found in the LUT-based LAI used with the USGS land-use map.
2) Surface temperature (2 m) was much improved in the model by inputting MODIS products such as land use, LAI, and GVF in comparison with USGS land use and table-dependent LAI. There was also improvement in 5-cm soil moisture and temperature conditions among the MODIS-input-data experiments. Surface fluxes, especially the latent heat flux, were significantly improved with the new MODIS data despite the overestimation of the sensible heat flux. Analyses from the domain average using NWS, three AmeriFlux station sites, and 10 IHOP_2002 station data sites suggested significant improvement in surface fluxes, 2-m temperature, and 5-cm soil temperature in all experiments conducted using MODIS land data products.
3) Significant differences were found between the two canopy-resistance approaches when MODIS products were used with the WRF–Noah coupled system. The Noah–GEM scheme estimated a nearly 60 $W\,m^{-2}$ lower latent heat flux whereas close agreement is found using Noah–Jarvis; slightly higher sensible heat fluxes were noted, however. Some degree of improvement was noted in the mixing ratio at the surface as well as in the ABL when MODIS products were applied. In addition, while there is growing evidence that the default Noah model ought to be replaced by a more interactive photosynthesis-based R_c scheme, this investigation suggests that recalibration of the Jarvis-type model from the in situ and satellite datasets improved surface parameters while the Noah–GEM scheme further improved mixing ratio, wind speed, and relative humidity in the ABL. These results also indicate that additional model changes are needed in the coupled mode to utilize better the remotely sensed land products and the improvements in the land surface physics from offline models. That is, the model coupling needs to be investigated more closely to benefit from the improvements in the land models being transferred to the atmospheric model.
4) The model physics determine the partitioning of the surface energy budget. This analysis clearly showed some experiments simulating latent heat values that

TABLE 5. Domain-averaged total precipitation from experiments and compared with observed stage-IV precipitation.

Simulated expt	Total precipitation (mm)
EXPT-1	19.83
EXPT-2	18.85
EXPT-3	17.20
EXPT-4	17.33
EXPT-5	17.85
EXPT-6	17.50
Obs	12.45

were close to those observed, but at the same time the sensible heat flux diverged from the observed value. Moreover, experiments designed with the new MODIS data improved latent heat flux but produced higher sensible heat flux. This problem can be overcome by using the Noah–GEM photosynthesis-based plant transpiration R_c scheme. Again, this warrants a deeper look into the input parameters provided within the Noah model and GEM scheme, because many parameters (coefficients and vegetation-dependent initialized parameters) have inherent uncertainty. At this time, the model is tuned to specific input parameters under an optimized environment, and hence more testing and optimization on these input parameters need to be completed.

5) The quantitative analysis in the boundary layer suggested that the MODIS data showed improvements in boundary layer moisture and wind speed, which are crucial parameters in determining cloud formation location. The new R_c scheme showed good agreement for mixing ratio, wind speed, and relative humidity but gave relatively large biases in the temperature of the atmospheric boundary layer. The resolved precipitation in the simulations was also improved with the experiments that were based on MODIS input data.

With these findings from the six designed experiments, the scope of land surface data from the MODIS satellite can be more clearly understood. With the increasing number of satellite datasets that offer high resolution in both space and time, such datasets are expected to be widely used in weather and climate modeling studies in the future. First, a significant difference in the results was seen when the USGS land-use map was replaced with the MODIS land-use map. With this change, improvements were seen in both surface fluxes and temperature and soil parameters. All of these components describe the land surface processes that influence evapotranspiration and determine the evolution of the boundary layer. Second, GVF and LAI are two important satellite products that, at high resolution in space and time, can represent more realistic surface conditions. Surface flux partitioning in the model was not balanced correctly in any of these experiments. Despite this result, improvements were noted in latent heat flux but with overestimated sensible heat. Even using a more detailed transpiration scheme coupled with WRF–Noah failed to capture the correct surface partitioning. Another issue arises when Noah–GEM input parameters are not provided accurately. Leaf temperature, for instance, can be estimated by providing surface temperature as the input since the current land model lacks such surface information. From the literature, it is known that there are several degrees of difference between leaf temperature and near-surface temperature, and therefore conducting further simulations using the Noah–GEM model coupled with a multilayer canopy model within the WRF modeling system, along with more robust evaluations of Noah–GEM, is suggested (Charusombat et al. 2010). Indeed, the ingestion of MODIS-based land surface conditions has a marked improvement in the overall coupled model performance, and this improvement can be further enhanced with better physics in the model.

Acknowledgments. This work was supported in part by the National Environmental Satellite, Data, and Information Service (NESDIS), NOAA/JCSDA (Research Area: Land Surface), DOE ARM (08ER64674; Dr. Rick Petty), NASA/GWEC-Terrestrial Hydrology Program (Dr. Jared Entin), and the NCAR Water Cycle Program. We also thank K. Manning (NCAR) and M. Duda (NCAR) for helping us with using satellite data in the model.

REFERENCES

Alfieri, J. G., D. Niyogi, P. D. Blanken, F. Chen, M. A. LeMone, K. E. Mitchell, M. B. Ek, and A. Kumar, 2008: Estimation of the minimum canopy resistance for croplands and grasslands using data from the 2002 International H_2O Project. *Mon. Wea. Rev.,* **136,** 4452–4469, doi:10.1175/2008MWR2524.1.

——, ——, H. Zhang, M. A. LeMone, and F. Chen, 2009: Quantifying the spatial variability of surface flux measurements using data from the International H_2O Project 2002: Linkages between surface conditions and spatial variability. *Bound.-Layer Meteor.,* **133,** 323–341, doi:10.1007/s10546-009-9406-2.

Baldocchi, D., 1992: A Lagrangian random-walk model for simulating water vapor, CO_2, and sensible heat flux densities and scalar profiles over and within a soybean canopy. *Bound.-Layer Meteor.,* **61,** 113–144, doi:10.1007/BF02033998.

Ball, J. T., I. E. Woodrow, and J. A. Berry, 1987: A model predicting stomatal conductance and its contribution to the control of photosynthesis under different environmental conditions. *Progress in Photosynthesis Research,* I. Biggins, Ed., Martinus Nijhoff, 221–224.

Barlage, M., X. Zeng, H. Wei, and K. E. Mitchell, 2005: A global 0.05° maximum albedo dataset of snow-covered land based on MODIS observations. *Geophys. Res. Lett.,* **32,** L17405, doi:10.1029/2005GL022881.

Beljaars, A. C. M., P. Viterbo, M. Miller, and A. Betts, 1996: The anomalous rainfall over the United States during July 1993: Sensitivity to land surface parameterization and soil moisture anomalies. *Mon. Wea. Rev.,* **124,** 362–383, doi:10.1175/1520-0493(1996)124<0362:TAROTU>2.0.CO;2.

Betts, A. K., 1986: A new convective adjustment scheme. Part I: Observational and theoretical basis. *Quart. J. Roy. Meteor. Soc.,* **112,** 677–691.

——, and M. J. Miller, 1986: A new convective adjustment scheme. Part II: Single column tests using GATE wave, BOMEX, and arctic air-mass data sets. *Quart. J. Roy. Meteor. Soc.,* **112,** 693–709, doi:10.1002/qj.49711247308.

——, F. Chen, K. E. Mitchell, and Z. I. Janjić, 1997: Assessment of land-surface and boundary-layer models in two operational versions of the Eta Model using FIFE data. *Mon. Wea. Rev.,* **125,** 2896–2915, doi:10.1175/1520-0493(1997)125<2896:AOTLSA>2.0.CO;2.

Boston University, 2012: User guide for the MODIS land cover type product. Land Cover and Surface Climate Group Doc., 5 pp. [Available online at http://www.bu.edu/lcsc/files/2012/08/MCD12Q1_user_guide.pdf.]

Buckley, T. N., K. A. Mott, and G. D. Farquhar, 2003: A hydromechanical and biochemical model of stomatal conductance. *Plant Cell Environ.,* **26,** 1767, doi:10.1046/j.1365-3040.2003.01094.x.

Calvet, J.-C., J. Noilhan, J. Roujean, P. Bessemoulin, M. Cabelguenne, A. Olioso, and J. Wigneron, 1998: An interactive vegetation SVAT model tested against data from six contrasting sites. *Agric. For. Meteor.,* **92,** 73–95, doi:10.1016/S0168-1923(98)00091-4.

Case, J. L., S. V. Kumar, J. Srikishen, and G. J. Jedlovec, 2011: Improving numerical weather predictions of summertime precipitation over the southeastern United States through a high-resolution initialization of the surface state. *Wea. Forecasting,* **26,** 785–807, doi:10.1175/2011WAF2222455.1.

Chang, H., D. Niyogi, A. Kumar, C. Kishtawal, J. Dudhia, F. Chen, U. C. Mohanty, and M. Shepherd, 2009: Possible relation between land surface feedback and the post-landfall structure of monsoon depression. *Geophys. Res. Lett.,* **36,** L15826, doi:10.1029/2009GL037781.

Charusombat, U., D. Niyogi, A. Kumar, X. Wang, F. Chen, A. Guenther, A. Turnipseed, and K. Alapaty, 2010: Evaluating a new deposition velocity module in the Noah land surface model. *Bound.-Layer Meteor.,* **137,** 271–290, doi:10.1007/s10546-010-9531-y.

Chen, F., and J. Dudhia, 2001a: Coupling an advanced land surface–hydrology model with the Penn State–NCAR MM5 modeling system. Part I: Model implementation and sensitivity. *Mon. Wea. Rev.,* **129,** 569–585, doi:10.1175/1520-0493(2001)129<0569:CAALSH>2.0.CO;2.

——, and ——, 2001b: Coupling an advanced land surface–hydrology model with the Penn State–NCAR MM5 modeling system. Part II: Preliminary model validation. *Mon. Wea. Rev.,* **129,** 587–604, doi:10.1175/1520-0493(2001)129<0587:CAALSH>2.0.CO;2.

——, K. Mitchell, J. Schaake, Y. Xue, H.-L. Pan, V. Koren, Q. Y. Duan, M. Ek, and A. Betts, 1996: Modeling of land surface evaporation by four schemes and comparison with FIFE observations. *J. Geophys. Res.,* **101,** 7251–7268, doi:10.1029/95JD02165.

——, Z. Janjić, and K. Mitchell, 1997: Impact of atmospheric surface layer parameterization in the new land-surface scheme of the NCEP mesoscale Eta numerical model. *Bound.-Layer Meteor.,* **85,** 391–421, doi:10.1023/A:1000531001463.

——, D. N. Yates, H. Nagai, M. A. LeMone, K. Ikeda, and R. L. Grossman, 2003: Land surface heterogeneity in the Cooperative Atmosphere Surface Exchange Study (CASES-97). Part I: Comparing modeled surface flux maps with surface-flux tower and aircraft measurements. *J. Hydrometeor.,* **4,** 196–218, doi:10.1175/1525-7541(2003)4<196:LSHITC>2.0.CO;2.

Collatz, J., J. Ball, C. Grivet, and J. Berry, 1991: Physiological and environmental regulation of stomatal conductance, photosynthesis and transpiration: A model that includes a laminar boundary layer. *Agric. For. Meteor.,* **54,** 107–136, doi:10.1016/0168-1923(91)90002-8.

——, M. Ribas-Carbo, and J. Berry, 1992: Coupled photosynthesis–stomatal conductance model for leaves of C4 plants. *Aust. J. Plant Physiol.,* **19,** 519–538, doi:10.1071/PP9920519.

Cox, P., R. Betts, C. Bunton, R. Esser, P. Rowntree, and J. Smith, 1999: The impact of new land surface physics on the GCM simulation of climate and climate sensitivity. *Climate Dyn.,* **15,** 183–203, doi:10.1007/s003820050276.

Dirmeyer, P. A., D. Niyogi, N. de Noblet-Ducoudré, R. E. Dickinson, and P. K. Snyder, 2010: Impacts of land use change on climate. *Int. J. Climatol.,* **30,** 1905–1907, doi:10.1002/joc.2157.

Dudhia, J., 1989: Numerical study of convection observed during the Winter Monsoon Experiment using a mesoscale two-dimensional model. *J. Atmos. Sci.,* **46,** 3077–3107, doi:10.1175/1520-0469(1989)046<3077:NSOCOD>2.0.CO;2.

Eastman, J. L., M. B. Coughenour, and R. A. Pielke Sr., 2001: The regional effects of CO_2 and landscape change using a coupled plant and meteorological model. *Global Change Biol.,* **7,** 797–815, doi:10.1046/j.1354-1013.2001.00411.x.

Ek, M., and L. Mahrt, 1991: A formulation for boundary-layer cloud cover. *Ann. Geophys.,* **9,** 716–724.

——, K. E. Mitchell, Y. Lin, E. Rogers, P. Grummann, V. Koren, G. Gayno, and J. D. Tarpley, 2003: Implementation of Noah land-surface model advances in the NCEP operational mesoscale Eta Model. *J. Geophys. Res.,* **108,** 8851, doi:10.1029/2002JD003296.

Farquhar, G. D., S. von Caemmerer, and J. Berry, 1980: A biochemical model of photosynthetic CO_2 assimilation in leaves of C3 species. *Planta,* **149,** 78–90, doi:10.1007/BF00386231.

Friedl, M. A., and Coauthors, 2002: Global land cover mapping from MODIS: Algorithms and early results. *Remote Sens. Environ.,* **83,** 287–302, doi:10.1016/S0034-4257(02)00078-0.

Gobron, N., A. Belward, B. Pinty, and W. Knorr, 2010: Monitoring biosphere vegetation 1998–2009. *Geophys. Res. Lett.,* **37,** L15402, doi:10.1029/2010GL043870.

Holt, T., D. Niyogi, F. Chen, M. A. LeMone, K. Manning, and A. L. Qureshi, 2006: Effect of land–atmosphere interactions on the IHOP 24–25 May 2002 convection case. *Mon. Wea. Rev.,* **134,** 113–133, doi:10.1175/MWR3057.1.

Hong, S., V. Lakshmi, and E. E. Small, 2007: Relationship between vegetation biophysical properties and surface temperature using multi-sensor satellite data. *J. Climate,* **20,** 5593–5606, doi:10.1175/2007JCLI1294.1.

Hong, S.-Y., and H.-L. Pan, 1996: Nonlocal boundary layer vertical diffusion in a medium-range forecast model. *Mon. Wea. Rev.,* **124,** 2322–2339, doi:10.1175/1520-0493(1996)124<2322:NBLVDI>2.0.CO;2.

——, and J.-O. J. Lim, 2006: The WRF single-moment 6-class microphysics scheme (WSM6). *J. Korean Meteor. Soc.,* **42,** 129–151.

——, J. Dudhia, and S. H. Chen, 2004: A revised approach to microphysical processes for the bulk parameterization of cloud and precipitation. *Mon. Wea. Rev.,* **132,** 103–120, doi:10.1175/1520-0493(2004)132<0103:ARATIM>2.0.CO;2.

Jacquemin, B., and J. Noilhan, 1990: Sensitivity study and validation of a land surface parameterization using the HAPEX-MOBILHY data set. *Bound.-Layer Meteor.,* **52,** 93–134, doi:10.1007/BF00123180.

Knote, C., G. Bonafe, and F. Di Giuseppe, 2009: Leaf area index specification for use in mesoscale weather prediction systems. *Mon. Wea. Rev.,* **137,** 3535–3550, doi:10.1175/2009MWR2891.1.

Kumar, A., F. Chen, D. Niyogi, J. Alfieri, M. Ek, and K. Mitchell, 2011: Evaluation of a photosynthesis-based canopy resistance

formulation in the Noah land-surface model. *Bound.-Layer Meteor.,* **138,** 263–284, doi:10.1007/s10546-010-9559-z.

Leese, J., T. Jackson, A. Pitman, and P. Dirmeyer, 2001: GEWEX/BAHC International Workshop on Soil Moisture Monitoring, Analysis, and Prediction for Hydrometeorological and Hydroclimatological Applications. *Bull. Amer. Meteor. Soc.,* **82,** 1423–1430, doi:10.1175/1520-0477(2001)082<1423:MSGBIW>2.3.CO;2.

LeMone, M. A., and Coauthors, 2007: NCAR/CU surface, soil, and vegetation observations during the International H_2O Project 2002 field campaign. *Bull. Amer. Meteor. Soc.,* **88,** 65–81, doi:10.1175/BAMS-88-1-65.

——, M. Tewari, F. Chen, J. G. Alfieri, and D. Niyogi, 2008: Evaluation of the Noah land surface model using data from a fair-weather IHOP_2002 day with heterogeneous surface fluxes. *Mon. Wea. Rev.,* **136,** 4915–4941, doi:10.1175/2008MWR2354.1.

Leuning, R., 1995: A critical appraisal of a combined stomatal-photosynthesis model for C3 plants. *Plant Cell Environ.,* **18,** 339–355, doi:10.1111/j.1365-3040.1995.tb00370.x.

Liu, Z., M. Notaro, J. Kutzbach, and N. Liu, 2006: Assessing global vegetation–climate feedbacks from observations. *J. Climate,* **19,** 787–814, doi:10.1175/JCLI3658.1.

Mahrt, L., and M. Ek, 1984: The influence of atmospheric stability on potential evaporation. *J. Climate Appl. Meteor.,* **23,** 222–234, doi:10.1175/1520-0450(1984)023<0222:TIOASO>2.0.CO;2.

——, and H. L. Pan, 1984: A two-layer model of soil hydrology. *Bound.-Layer Meteor.,* **29,** 1–20, doi:10.1007/BF00119116.

Medlyn, B. E., and Coauthors, 2001: Stomatal conductance of forest species after long-term exposure to elevated to CO_2 concentration: A synthesis. *New Phytol.,* **149,** 247–264, doi:10.1046/j.1469-8137.2001.00028.x.

Miller, J., M. Barlage, X. Zeng, H. Wei, K. Mitchell, and D. Tarpley, 2006: Sensitivity of the NCEP/Noah land surface model to the MODIS green vegetation fraction data set. *Geophys. Res. Lett.,* **33,** L13404, doi:10.1029/2006GL026636.

Mitchell, K., H. Wei, S. Lu, G. Gayno, and J. Meng, 2005: NCEP implements major upgrade to its medium-range Global Forecast System, including land-surface component. *GEWEX News,* Vol. 15, No. 4, International GEWEX Project Office, Silver Spring, MD, 8–9. [Available online at http://www.gewex.org/Nov2005.pdf.]

Mlawer, E. J., S. J. Taubman, P. D. Brown, M. J. Iacono, and S. A. Clough, 1997: Radiative transfer for inhomogeneous atmosphere: RRTM, a validated correlated-*k* model for the longwave. *J. Geophys. Res.,* **102,** 16 663–16 682, doi:10.1029/97JD00237.

Mostovoy, G., V. Anantharaj, R. King, and M. Filippova, 2008: Interpretation of the relationship between skin temperature and vegetation fraction: Effect of subpixel soil temperature variability. *Int. J. Remote Sens.,* **29,** 2819–2831, doi:10.1080/01431160701395286.

Nikolov, N. T., W. J. Massman, and A. W. Shoettle, 1995: Coupling biochemical and biophysical processes at the leaf level: An equilibrium photosynthesis model for leaves of C3 plants. *Ecol. Modell.,* **80,** 205–235, doi:10.1016/0304-3800(94)00072-P.

Niyogi, D., and S. Raman, 1997: Comparison of four different stomatal resistance schemes using FIFE observations. *J. Appl. Meteor.,* **36,** 903–917, doi:10.1175/1520-0450(1997)036<0903:COFDSR>2.0.CO;2.

——, T. Holt, S. Zhong, P. C. Pyle, and J. Basara, 2006: Urban and land surface effects on the 30 July 2003 mesoscale convective system event observed in the southern Great Plains. *J. Geophys. Res.,* **111,** D19107, doi:10.1029/2005JD006746.

——, H. Chang, F. Chen, L. Gu, A. Kumar, S. Menon, and R. A. Pielke Sr., 2007: Potential impacts of aerosol–land–atmosphere interaction on the Indian monsoonal rainfall characteristics. *Nat. Hazards,* **42,** 345–359, doi:10.1007/s11069-006-9085-y.

——, K. Alapaty, S. Raman, and F. Chen, 2009: Development and evaluation of a coupled photosynthesis-based Gas Exchange Evapotranspiration Model (GEM) for mesoscale weather forecasting applications. *J. Appl. Meteor.,* **48,** 349–368, doi:10.1175/2008JAMC1662.1.

Noilhan, J., and S. Planton, 1989: A simple parameterization of land surface processes for meteorological models. *Mon. Wea. Rev.,* **117,** 536–549, doi:10.1175/1520-0493(1989)117<0536:ASPOLS>2.0.CO;2.

Pan, H.-L., and L. Mahrt, 1987: Interaction between soil hydrology and boundary layer development. *Bound.-Layer Meteor.,* **38,** 185–202, doi:10.1007/BF00121563.

Pielke, R. A., Sr., and Coauthors, 2011: Land use/land cover changes and climate: Modeling analysis and observational evidence. *Wiley Interdiscip. Rev.: Climate Change,* **2,** 828–850, doi:10.1002/wcc.144.

Pitman, A. J., 2003: The evolution of, and revolution in, land surface schemes designed for climate models. *Int. J. Climatol.,* **23,** 479–510, doi:10.1002/joc.893.

Robock, A., K. Y. Vinnikov, G. Srinivasan, J. K. Entin, S. E. Hollinger, N. A. Speranskaya, S. Liu, and A. Namkhai, 2000: The global soil moisture data bank. *Bull. Amer. Meteor. Soc.,* **81,** 1281–1299, doi:10.1175/1520-0477(2000)081<1281:TGSMDB>2.3.CO;2.

Ronda, R. J., H. A. R. de Bruin, and A. A. M. Holtslag, 2001: Representation of the canopy conductance in modeling the surface energy budget for low vegetation. *J. Appl. Meteor.,* **40,** 1431–1444, doi:10.1175/1520-0450(2001)040<1431:ROTCCI>2.0.CO;2.

Rosero, E., Z.-L. Yang, T. Wagener, L. E. Gulden, S. Yatheendradas, and G.-Y. Niu, 2010: Quantifying parameter sensitivity, interaction, and transferability in hydrologically enhanced versions of the Noah land surface model over transition zones during the warm season. *J. Geophys. Res.,* **115,** D03106, doi:10.1029/2009JD012035.

Sellers, P. J., and Coauthors, 1996a: A revised land surface parameterization (SiB2) for atmospheric GCMs. Part I: Model formulation. *J. Climate,* **9,** 676–705, doi:10.1175/1520-0442(1996)009<0676:ARLSPF>2.0.CO;2.

——, S. O. Los, C. J. Tucker, C. O. Justice, D. A. Dazlich, G. J. Collatz, and D. A. Randall, 1996b: A revised land surface parameterization (SiB2) for atmospheric GCMs. Part II: The generation of global fields of terrestrial biophysical parameters from satellite data. *J. Climate,* **9,** 706–737, doi:10.1175/1520-0442(1996)009<0706:ARLSPF>2.0.CO;2.

Shin, H. H., S.-Y. Hong, and J. Dudhia, 2012: Impacts of the lowest model level height on the performance of planetary boundary layer parameterizations. *Mon. Wea. Rev.,* **140,** 664–682, doi:10.1175/MWR-D-11-00027.1.

Skamarock, W. C., J. B. Klemp, J. Dudhia, D. O. Gill, D. M. Barker, W. Wang, and J. G. Powers, 2005: A description of the Advanced Research WRF version 2. NCAR Tech. Note NCAR/TN–468+STR, 88 pp. [Available online at http://www.mmm.ucar.edu/wrf/users/docs/arw_v2.pdf.]

Trier, S. B., and C. A. Davis, 2005: Propagating nocturnal convection within a 7-day WRF model simulation. *Proc. 11th Conf. on Mesoscale Processes,* Albuquerque, NM, Amer.

Meteor. Soc., 10.6. [Available online at https://ams.confex.com/ams/pdfpapers/97323.pdf.]

Vivoni, E. R., H. A. Moreno, G. Mascaro, J. C. Rodrıguez, C. J. Watts, J. Garatuza Payan, and R. Scott, 2008: Observed relation between evapotranspiration and soil moisture in the North American monsoon region. *Geophys. Res. Lett.,* **35,** L22403, doi:10.1029/2008GL036001.

Wang, Z., X. Zeng, and M. Barlage, 2007: Moderate Resolution Imaging Spectroradiometer bidirectional reflectance distribution function–based albedo parameterization for weather and climate models. *J. Geophys. Res.,* **112,** D02103, doi:10.1029/2005JD006736.

Weckwerth, T., and Coauthors, 2004: An overview of the International H_2O Project (IHOP 2002) and some preliminary highlights. *Bull. Amer. Meteor. Soc.,* **85,** 253–277, doi:10.1175/BAMS-85-2-253.

Wei, M.-Y., Ed., 1995: Soil moisture: Report of a workshop held in Tiburon, California, 25-27 January 1994. NASA Conference Publ. 3319, 80 pp. [Available online at https://ia600605.us.archive.org/25/items/nasa_techdoc_19960016993/19960016993.pdf.]

Wood, E. F., and Coauthors, 1998: The Project For Intercomparison of Land-Surface Parameterization Schemes (PILPS Phase 2(c)) Red-Arkansas River basin experiment: 1. Experiment description and summary intercomparisons. *Global Planet. Change,* **19,** 115–135, doi:10.1016/S0921-8181(98)00044-7.

Zhan, X., Y. K. Xue, and G. J. Collatz, 2003: An analytical approach to estimating CO_2 and heat fluxes over the Amazonian region. *Ecol. Modell.,* **162,** 97–117, doi:10.1016/S0304-3800(02)00405-2.